Head-to-tail interactions of the coiled-coil domains regulate ClpB cooperation with Hsp70 in protein disaggregation

Marta Carroni, Eva Kummer, Yuki Oguchi, Petra Wendler, Daniel K Clare, Irmgard Sinning, Jürgen Kopp, Axel Mogk, Bernd Bukau, Helen Saibil

DOI: http://dx.doi.org/10.7554/eLife.02481

Cite as: eLife 2014;10.7554/eLife.02481

Received: 6 February 2014
Accepted: 29 April 2014
Published: 30 April 2014

Head-to-tail interactions of the coiled-coil domains regulate ClpB activity and cooperation with Hsp70 in protein disaggregation

Marta Carroni[1], Eva Kummer[2], Yuki Oguchi[2], Petra Wendler[3], Daniel K. Clare[1], Irmgard Sinning[4], Jürgen Kopp[4], Axel Mogk[2], Bernd Bukau[2] and Helen R. Saibil[1,a]

1. Department of Crystallography, Birkbeck College, London, UK.
2. Zentrum für Molekulare Biologie der Universität Heidelberg, Heidelberg, Germany.
3. Gene Center, Ludwig-Maximilians-University Munich, 81377 Munich, Germany
4. Biochemie-Zentrum der Universität Heidelberg (BZH), Im Neuenheimer Feld 328, Heidelberg D-69120, Germany

a) Corresponding author: h.saibil@mail.cryst.bbk.ac.uk

Abstract

The hexameric AAA+ chaperone ClpB reactivates aggregated proteins in cooperation with the Hsp70 system. Essential for disaggregation, the ClpB middle domain (MD) is a coiled-coil propeller that binds Hsp70. Although the ClpB subunit structure is known, positioning of the MD in the hexamer and its mechanism of action are unclear. We obtained electron microscopy (EM) structures of the BAP variant of ClpB that binds the protease ClpP, clearly revealing MD density on the surface of the ClpB ring. Mutant analysis and asymmetric reconstructions show that MDs adopt diverse positions in a single ClpB hexamer. Adjacent, horizontally oriented MDs form head-to-tail contacts and repress ClpB activity by preventing Hsp70 interaction. Tilting of the MD breaks this contact, allowing Hsp70 binding, and releasing the contact in adjacent subunits. Our data suggest a wavelike activation of ClpB subunits around the ring.

Introduction

Cellular machinery has evolved to prevent or reverse protein misfolding and aggregation, which are damaging to cells and tissues. Bacterial ClpB and its yeast counterpart Hsp104 are members of the Clp/Hsp100 family and function in disaggregation and refolding of protein aggregates together with Hsp70 and its co-chaperones [1-6]. ClpB/Hsp104 are conserved in bacteria, fungi, plants and

mitochondria and are essential for recovery of cells from heat shock and other proteotoxic stresses [7,8]. The oligomeric ring Hsp100 proteins thread substrates through a central channel, via binding to conserved tyrosine residues on flexible loops [9-14]. They belong to the AAA+ (ATPases associated with various cellular activities) superfamily of ATPases, with characteristic α and β subdomains [15,16]. ATP binds between the two subdomains and at the subunit interface of adjacent monomers, with a catalytic Arg-finger provided by the neighbouring subunit.

While some other members of the Hsp100 family have been crystallised in their oligomeric form [17-19], the atomic structure of ClpB is known only for the monomer (*T. thermophilus*). ClpB is composed of a N-terminal domain (ND) followed by two AAA+ domains (AAA-1 and AAA-2). An 85 Å long coil-coiled propeller, the middle domain (MD), is inserted into the small subdomain of AAA-1 [20]. It has two blades with mutationally sensitive sites at either end, termed motif 1 and motif 2. Cryo-EM reconstructions of *Tth*ClpB hexamers show a two-tiered molecule accounting for the AAA+ rings, but lack density for the ND. On the other hand, various cryo-EM studies of Hsp104 revealed the presence of an ND ring on top of the AAA+ ones. Although the overall shape and dimensions of the ClpB and Hsp104 hexamers are comparable in the various cryo-EM studies, there are substantial differences in the channel width [20-23]. Observation of narrow [20,21] (15 to 30 Å) versus expanded [22,23] (30 to 80 Å) cavities has led to different pseudo-atomic models of the hexamers. In one model, the AAA+ rings are compact, as in the crystal structures of other AAA+ hexamers such as p97, HslU or SV40 LTag, with the Arg-finger contacting the neighbouring subunit [17,24,25]. In the EM maps used to build this compact model there is little or no density for the MD and it was assumed to extend radially outwards from the ring [20,21]. In the expanded model, the AAA+ domains are more widely separated with the MD intercalated between them, preventing the canonical Arg-finger contacts [22,23]. An attempt to localize the Hsp104 MD by genetically inserting a lysozyme resulted in a cryo-EM reconstruction of this chimera with visible density for the lysozyme, but not for the MD itself [21]. Since none of the existing cryo-EM structures allows an unambiguous localization of the MD, its position is still a matter of debate [26].

The MD confers unique disaggregase ability to ClpB/Hsp104 [27,28] and is required for species-specific cooperation with the DnaK-DnaJ(DnaKJ)/Hsp70-Hsp40 system [29-31]. A direct interaction between the ClpB MD and DnaK has been shown by NMR

spectroscopy and site-specific crosslinking and involves the motif 2 tip of the MD and the ATPase domain of DnaK [30,32]. The MD acts to repress ClpB disaggregase activity, and DnaK binding relieves this repression [30,33]. Point mutations in the MD show that interactions between motif 2 and AAA-1 are critical for regulating ATPase and disaggregase activities [30,33-35]. Thus, the MD plays an essential role in coupling Hsp70 interaction to ATPase regulation and substrate disaggregation in ClpB/Hsp104. It is therefore important to understand its structural role in ClpB/Hsp104 hexamers and in the context of the ClpB-DnaKJ bi-chaperone machinery.

To address the ambiguities in domain arrangement and to elucidate the working principle of the MD, we performed single particle EM studies of ClpB under conditions where its orientation could be determined more reliably than in previous studies. We used BAP (ClpB with the ClpA tripeptide for ClpP binding), a chimera engineered to bind the ClpP protease via the replacement of a C-terminal ClpB segment with the ClpP binding region of ClpA [14]. This construct has been extensively used to study the ClpB disaggregation mechanism by monitoring substrate proteolysis after delivery to ClpP [9,12,14,32,36] (Figure 1A). Therefore, BAP is suitable for structural studies and has allowed us to obtain maps with visible MD densities that shed light on its regulatory mechanisms.

Results

Three-dimensional (3D) reconstruction of negatively stained BAP-ClpP shows clear density for the middle domain

Using the BAP complex facilitates orientation determination in EM reconstruction, as previously observed for ClpA-ClpP [37]. Side views of the elongated BAP-ClpP complex are easily recognisable (Figure 1B) whereas in 2D projections of ClpB alone, which has a globular shape, it is hard to distinguish side from tilted views. By restricting the dataset to side views the angle assignment is more reliable, and these views are sufficient to generate the full 3D structure (Figure 1C). Using H/D exchange experiments, which report on the solvent accessibility and structural flexibility of amide hydrogens, we found that BAP, either alone or bound to ClpP, displays the same protection pattern as ClpB, implying the same MD conformation (Figure 1-supplement 1).

The BAP-ClpP complexes formed by mixing BAP and ClpP at a 1:1 molar ratio of hexamer to heptamer in the presence of ATPγS were stained with uranyl acetate. Complexes containing two BAP hexamers per ClpP double-heptamer were picked for single particle analysis and separated into halves for processing [37] (Figure 1B). Initial analysis revealed the presence of four layers corresponding to the ND, AAA-1, AAA-2 and ClpP rings. Class averages and eigenimage analysis indicate that the ND is extremely mobile in the BAP hexamer (Figure 1-supplement 2), consistent with crystallographic data on monomeric *T. thermophilus* ClpB [20]. The ND layer was therefore excluded during later stages of image alignment. Similarly, the region corresponding to ClpP, very useful for the initial analysis, was not included in the refinement because of its symmetry mismatch with ClpB. Using ~12,000 particles, we obtained a 3D map by refining the alignment of the two AAA+ rings only, but then including the whole molecule in the reconstruction, which was at ~17 Å resolution (Figure 1C,D; Figure 1-supplement 3). In order to simplify the problems of alignment and reconstruction, we initially imposed 6-fold symmetry, which blurs the features of the heptameric ClpP ring. Similarly, the mobile ClpB ND is blurred into a solid disc.

The BAP hexamer has overall outer dimensions of ~150 × 100 Å, similar to previous structures of ClpB/Hsp104 [20,22,23,38] (Figure 1C). It encloses a ~30 Å wide central channel, comparable in size to that in the crystal structure of ClpC [19] (Figure 1C,D). In the reconstruction it is possible to identify regions accounting for all the domains, such as L-shaped densities for the AAA+ domains and a rod-like density for the coiled-coil MD.

To interpret the domain interactions, we fitted ClpB atomic coordinates into the EM density. We determined the crystal structure of an ND truncation of *E. coli* ClpB (residues 159 to 858; E432A mutation; Table 1). The subunit structure is very similar to that of *T. thermophilus* ClpB (Figure 1-supplement 4). Since none of the available crystal structure conformations fit in the EM map, domains were fitted as separate rigid bodies connected at hinge regions (Figure 1C). For the AAA-1 ring, it was possible to build a hexamer model based on the crystal structure of hexameric ClpC [19] (PDB code 3PXG), a homologue that also displays disaggregation activity *in vitro* [39]. The resulting ClpB AAA-1 hexamer model was automatically docked into the AAA-1 layer as a rigid body (Figure 1D). This strategy was chosen over the fitting of a single subunit followed by hexamerisation because it is expected to provide a more accurate

picture of the subunit interface, which is difficult to determine at the resolution of our EM map. However, this approach did not work for the AAA-2 layer since the ClpB AAA-2 hexamer based on the ClpC crystal structure was not compatible with the density. In this case a ~40° tilt of the monomers into the plane of the ring was required to obtain the optimal fit, which resembles the pseudo-atomic model of the homologue ClpA AAA-2 ring [37]. Coordinates of the *E. coli* ClpB ND (residues 1 to 148) were obtained from the PDB (1KHY). A single N domain was fitted manually, maintaining the connection to AAA-1, and then hexamerised by applying symmetry in Chimera [58].

The AAA+ rings have a central opening of ~30 Å and therefore are not as compact as in one of the previous models [20,21,40], but not as expanded as in the other [22]. The Arg-fingers are at the interface between subunits, available to catalyse hydrolysis as expected from mutational studies [28,41,42].

The ClpB coiled-coil MDs were separately docked in the rod-shaped densities surrounding the AAA-1 ring (Figure 3D), maintaining the connection to the AAA-1 small subdomain. The pseudo-atomic model of one ClpB subunit obtained from this fitting differs from the crystal structure by rotations about the inter-domain hinge points (Figure 1-supplement 4B).

In this position, the MD contacts the neighbouring AAA-1 via its motif 1, while motif 2 makes intrasubunit AAA-1 interactions. This is in good agreement with recent biochemical data showing protection of these two motifs upon ClpB oligomerisation and formation of an intermolecular disulphide bond between E344C of AAA-1 and L424C of a neighboring MD motif 1 [33] (Figure 1E).

Moreover, intramolecular disulphide cross-links engineered between AAA-1 and motif 2 residues in *Tth*ClpB, *Eco*ClpB and yeast Hsp104 are also compatible with the fitted structure (Figure 1E; K476C/E358C [33]; G175C/R484C, H362C/Q473C *E. coli* numbering [20]; G175C/S499C [34]; Hsp104 K358C/D484C [35]). However, this arrangement is not compatible with some of the engineered disulphide bonds observed in yeast Hsp104 [43] (D427C/E475C, D427C/E471C and E320C/N467C).

To investigate possible species-specific structural differences we reconstructed the functional yeast homologue HAP (Hsp104 with the ClpA tripeptide for ClpP binding) in complex with ClpP. Using ~10,000 particles and analyzing the data as described above, an independent map of HAP was obtained at ~21 Å resolution (Figure 2A; Figure 1-supplement 3). The three-layered structure is comparable to BAP and there is density accounting for all domains including the MD, which surrounds the AAA-1 ring. The atomic coordinates of the ND and AAA+ rings obtained from the BAP analysis were fitted as rigid bodies. In order to fit the density, the MD must adopt a more horizontal orientation (Figure 2A). In summary, HAP shows overall the same structural organisation as its bacterial homologue ClpB.

Cryo EM reconstructions of ClpB with and without ClpP support the negative stain maps

Since negative stain EM of ClpB (BAP) in complex with ClpP gave a clear result different from all previous cryo EM maps of ClpB and Hsp104, we collected cryo EM data on BAP-ClpP as well as on ClpB alone. The same strategy of using only clearly identifiable side views was applied. Complexes were imaged in the presence of ATPγS and independent maps were obtained by *de novo* angular reconstitution in each case (Figure 2B,C).

For cryo EM of the BAP-ClpP complex, we used a Trap (E279A/E678A) variant, which can bind but not hydrolyse ATP due to mutations in both Walker B motifs. We anticipated that the Trap construct would be more stable than the wild type, but data collection was challenging because side views were not abundant. Eventually, ~4500 particles were collected and the same processing strategy was used as for the negative stain data. This variant is more likely to trap non native substrates in its central channel, and the extra density seen in this complex is likely to arise from denatured protein, possibly ClpP, present in the sample (Figure 2B).

In the case of isolated ClpB, side views were sorted on the basis of multivariate statistical analysis (MSA). Briefly, particles representing all views of ClpB were picked, centered and classified by MSA. Only particles belonging to classes representing side-views ($80° < \beta < 100°$) were extracted and used for further processing.

Both maps show overall dimensions and density distributions comparable to the negative stain structure of BAP in complex with ClpP, confirming that the ClpB hexamer structure is not significantly altered either by negative staining or by binding to ClpP. The atomic model derived by fitting the negative stain BAP-ClpP map could

be docked as a rigid body into both cryo EM reconstructions, but the MD assumes a more horizontal orientation, similar to that in HAP (Figure 2).

ClpB activity mutants show altered MD orientations

E432A and Y503D are ClpB point mutations at opposite ends of the MD coiled-coil, which result in repressed (E432A) and hyperactive (Y503D) states [30,33]. Repressed ClpB-E432A is deficient in DnaK interaction and cannot be activated by its Hsp70 partner. Hyperactive ClpB-Y503D shows high ATPase and substrate unfolding activity even in the absence of Hsp70 [30,33]. We collected negative stain EM datasets of the BAP-ClpP complexes of these variants and obtained 3D reconstructions of BAP-E432A and BAP-Y503D at 18 Å and 20 Å, respectively (Figure 3; Figure 1-supplement 3). Starting models were independently (Figure 3-supplement 1) generated by angular reconstitution and refined with 6-fold symmetry. Both mutants assemble into three layers similar to the wild type and show high variability in the ND ring. Atomic coordinates of the AAA+ rings can be fitted as described for the wild type, using the ClpC hexamer as starting point. Some rearrangement was necessary to fit the ND into density (Figure 3). The most notable difference between the two maps is a ~30º difference in orientation of the motif 1 blade of the MD and the loss of the motif 2 density in the hyperactive state (Figure 4A,B). Another difference observed upon alignment of the AAA-1 ring in the repressed, wild-type and hyperactive maps is a ~15° rotation of the wild-type AAA-2 ring relative to the mutants.

In the BAP-E432A repressed mutant the MD is clearly visible around the AAA-1 ring. It has a horizontal orientation so that motif 2 forms a contact with motif 1 of the neighbouring MD (Figure 3B; Figure 4B). This packing of the MD is supported by biochemical data showing overprotection of motif 2 in this mutant [33]. Moreover, a very similar intersubunit motif 1-motif 2 contact is seen in all the ClpB crystal structures, in which ClpB monomers are arranged in a spiral assembly (*Tth*ClpB, 1QVR [20]; *Eco*ClpB current study) (Figure 4-supplement 1).

In the Y503D hyperactive form there is density for motif 1 in a more tilted orientation, but there is no density visible for motif 2, suggesting that this region becomes either disordered or highly mobile (Figure 3C,D). This finding is in accordance with H/D exchange data showing deprotection of this region in the BAP-Y503D mutant [33]. We conclude that, in the Y503D hyperactive form, the motif 1 arm

of the MD is tilted downwards so that it can no longer contact motif 2 of the adjacent MD, and binds to a lower region of the neighbouring AAA-1 domain. Motif 2 is mobile and solvent exposed (Figure 3C,D; Figure 4A,B).

Alignment of AAA-1 domains of wild type, repressed and hyperactive forms of ClpB/BAP confirms that the MD rotates ~30° from a tilted orientation in the hyperactive state, to a horizontal one in the repressed state, with the wild type occupying an intermediate orientation (Figure 4B). In this movement motif 1 switches from being protected against AAA-1 to engaging motif 2 in trans. These different orientations of the MD have opposite consequences for DnaK binding. The horizontal MD position, with motif 1 contacting motif 2 of the neighbouring subunit, is incompatible with DnaK binding at the tip of motif 2 [30,32]. In contrast, tilting of the MD exposes motif 2 for DnaK interaction.

To confirm the close proximity of motif 1 and motif 2 of neighbouring MDs we performed fluorescence resonance energy transfer (FRET) experiments using Q427W (motif 1) as FRET donor and IAEDANS labelled Q502C (motif 2) as FRET acceptor. The FRET pair (Förster radius of 22 Å) has a distance of 19.1 Å in the wild type model and was introduced into the tryptophan-free ClpB-W462Y/W543L variant. In addition we coupled the FRET pair to E432A and Y503D mutations, to monitor the consequences of repressed and hyperactive states on FRET efficiency. The distance between the FRET partners is either reduced (11.3 Å) or increased (35.9 Å) in models of the repressed and hyperactive variants, respectively (Figure 4B). All ClpB variants were IAEDANS labeled with similar efficiencies (70-80%; Figure 4-supplement 2). High IAEDANS fluorescence and thus FRET efficiency was observed for wild type ClpB and E432A upon ClpB oligomerization. Increase in acceptor fluorescence in general correlated with reduced tryptophan emission except for ClpB wild type upon oligomerization. In contrast, IAEDANS fluorescence remained low under all conditions tested when the FRET pair was linked to Y503D (Figure 4C).

Furthermore, to test for direct interaction between motif 1 and motif 2, we introduced cysteine residues into motif 1 (K431C) and motif 2 (S499C) and analyzed whether intermolecular crosslinks form under oxidizing conditions. Low Cu-Phenanthrolin concentrations (25 μM) yielded a ladder of crosslink products from ClpB dimers to hexamers. Although non-specific dimer formation was observed in single cysteine

variants, higher oligomers were only found in double cysteine variants (Figure 4D). Introducing the activating (Y503D) mutation to ClpB-K431C/S499C decreased but did not abolish crosslink formation, suggesting rapid fluctuation of MDs between different conformations even in the hyperactive state (Figure 4D). These findings support the interaction of MD motifs 1 and 2 from adjacent subunits as observed in the EM reconstructions and strengthening or loosening of the contact in repressed and hyperactive states, respectively.

Motif 1 is essential for keeping ClpB in the repressed state

Mutating MD motif 1 can impair Hsp70 interaction and consequently protein disaggregation [30,33]. On the other hand a ClpB motif 1 deletion variant retains substantial disaggregation activity [30,44], providing no clarification of its role in protein disaggregation. Our EM structural data indicate that motif 1 acts as a crucial component of ClpB regulation by stabilizing MDs in a horizontal position through interaction with an adjacent motif 2. Indeed, ClpB-ΔM1 (ΔE410-Y455) shows hyperstimulation of ATPase activity in the presence of the substrate casein compared to wild-type ClpB, resembling the deregulated ATPase activity of hyperactive ClpB variants lacking motif 2 or the entire MD [33] (Figure 5A). The basal ATPase activity of ClpB-ΔM1 was reduced in comparison to wild type due to partial oligomerization defects, in agreement with earlier reports [33,44]. ClpB-ΔM1 oligomerization defects were more pronounced than in ClpB-ΔM1/M2, suggesting that motif 2 in absence of motif 1 might impede hexamer formation.

Next we tested whether hyperstimulation of ATPase activity is linked to high unfolding power. We employed BAP variants of the respective deletion constructs and tested for unfolding and degradation of casein-YFP in presence of ClpP. BAP-ΔM1 unfolds the YFP moiety of casein-YFP, an activity only observed for hyperactive BAP variants but not wild type BAP [33] (Figure 5B). Loss of ClpB regulation in ClpB-ΔM1 was also linked to severe toxicity upon expression in *E. coli* Δ*clpB* mutant cells (Figure 5C). However, higher expression levels of ClpB-ΔM1 than of ClpB-Y503D are required to observe the same degree of toxicity probably because deletion of motif 1 results in oligomerisation defects [33] (Figure 5C). In conclusion ClpB-ΔM1 exhibits the three major characteristics of hyperactive ClpB variants (high ATPase and unfolding activities linked to cellular toxicity), demonstrating the crucial regulatory role for motif 1 in interacting with an adjacent motif 2 to ensure tight activity control of ClpB.

Asymmetric reconstructions show variable orientations of the MD around the ring

As mentioned above, we imposed 6-fold symmetry as a first approximation, to simplify the alignment and reconstruction problem. Nevertheless, crystal structures of the AAA+ protein ClpX show that the homo-hexameric assembly can be markedly asymmetric [18,45,46]. We therefore reanalysed our negative stain EM data without imposing symmetry, in order to study the conformational variability within the hexamer.

Using ~15,000, ~10,000 and ~9000 particles for wild-type BAP, BAP-E432A and BAP-Y503D we obtained asymmetric maps at 21 Å, 21 Å and 25 Å resolution, respectively (Figure 6A; Figure 1-supplement 3; Figure 6-supplement 1). Although the numbers of particles were similar to those used for 6-fold analysis, the resolution is only slightly worse and the maps are comparable in quality to the symmetrised ones, consistent with the structure being asymmetric. The structure of the hyperactive mutant is less defined and has lower resolution than the other two, particularly for the MDs, probably owing to their higher mobility. Therefore, only wild-type BAP and BAP-E432A were used for further analysis.

The asymmetric structures show similar density distributions in the AAA+ rings, even though not all six subunits in a ring can be aligned simultaneously owing to 5°-15° variations in rotational orientation. This rotational variability may explain the apparent ~15° rotation of the AAA-2 wild-type ring relative to the mutants observed in the symmetrised reconstructions. As expected from the eigenimage analysis, the ND ring is not very well defined and the density does not account for all six NDs. Therefore, we did not attempt any atomic structure fitting into this region. Docking of the atomic structures of AAA-1, AAA-2 and MD was performed as follows.

Structures of AAA+ proteins crystallised in their hexameric assemblies show that the large and small subdomains of the AAA fold assume a range of conformations that can be clustered into open or closed forms [46,47] (Figure 6-supplement 2). The closed conformation is ATP-binding competent and there are intermediate forms that might also represent weak binding states. Using a gallery of available AAA+ crystal structures we modelled open, closed and intermediate conformations of ClpB AAA-1 and AAA-2. We also created AAA+ dimers of adjacent ClpB subunits based on ClpX pseudo-hexameric crystal structures [18,46] (Figure 6-supplement 2) that were fitted as

rigid bodies into the asymmetric reconstructions. Crystallographic dimers are likely to provide more realistic models of subunit interfaces than can be deduced by fitting individual subunits into low-resolution maps.

The AAA-2 ring density could be almost entirely interpreted using this approach and the fit suggests that 3 to 5 subunits are sufficiently closed to bind ATP (Fig. 6-supplement 2). We analyzed nucleotide (ADP) binding to wild type ClpB by isothermal calorimetry (ITC) revealing a binding stoichiometry of 7.5 +/- 0.1 ADP per hexamer (Figure 6-supplement 3). ITC experiments using ClpB-K212A, which is deficient in nucleotide binding in AAA-1, allowed us to determine a binding stoichiometry of 3.7 +/- 0.3 ADP in AAA-2 of the mutant hexamer (Figure 6-supplement 3). The same ADP binding stoichiometry was also found for the repressed and hyperactive variants (Figure 6-supplement 3). The deduced stoichiometries are in good agreement with the distinct AAA-2 conformations observed in the asymmetric EM reconstructions. Similar calculations have been reported for the AAA+ proteins MCM, ClpX and HslU [48,49]. The AAA-1 ring is more asymmetric than AAA-2 and it is not easily interpretable by fitting crystallographic dimer models. There is sufficient density to guide rigid body fitting of all AAA-1 domains, but this fitting does not allow deductions of nucleotide occupancy (Figure 6-supplement 2).

Asymmetric reconstructions of both wild-type BAP and repressed mutant display clear densities accounting for the MDs that lie outside the AAA-1 ring and assume different orientations similar to those observed in the symmetrised maps of wild type and mutants. In the wild-type asymmetric reconstruction, the MD orientation ranges from horizontal as in the repressed state to highly tilted, similar to the hyperactive state, passing through the intermediate wild type-like state (Figure 6B). In one subunit, motif 1 contacts AAA-2 of the same subunit, suggesting a route of allosteric communication between AAA-1 and AAA-2. Additionally, this contact is compatible with recently reported engineered disulphide bonds between motif 1 residues and AAA-2 in Hsp104 and ClpB [43]. The tilted MDs are clustered together, consistent with the release of motif 1-motif 2 contacts, freeing adjacent subunits.

In the asymmetric reconstruction of the repressed state, five MDs are found in the horizontal orientation, followed by a sixth for which there is no clear density (Figure 6C). In the wild type two MDs can make the motif 1 to motif 2 contact, while

in the repressed state up to five MDs are compatible with this contact (Figure 6B,C). Conversely, in the wild type at least two MDs exist in a clearly activated state but in the repressed state none of the MDs are visible in the tilted, hyperactive conformation. As a consequence, the MD conformations in BAP-E432A do not support Hsp70 binding and ATPase activation, in agreement with previous findings [30,33]. However, ClpB wild type hexamers harbour two MDs that favour Hsp70 recruitment, potentially priming the ClpB ring for further activation.

Discussion

The BAP construct of ClpB complexed with ClpP, combined with a conservative approach of using only clearly identifiable side views and basing the analysis mainly on negative stain images (with independent confirmation from cryo EM) enabled us to unambiguously locate all subunit domains in the oligomer, including the coiled-coil MD propeller. Although the quoted resolutions for some previous structures of ClpB and Hsp104 were better, the globular shape, flexibility and asymmetry of these hexamers reduce the reliability of orientation assignment. Moreover, previous published structures of ClpB/Hsp104 were obtained by cryo EM only, which provides a lower signal-to-noise ratio (SNR) than negative stain data.

Rigid body fitting of *E. coli* ClpB atomic coordinates (PDB code 4CIU) into our new maps reveals that the MD is not projecting outwards from the hexamer [20,21,40] nor is intercalated between subunits [22,23], but is instead lying on the surface of the ClpB hexameric ring with a variable degree of tilt (Figure 4A; Figure 6B,C). A similar position of the MD is seen for Hsp104, underlining the conserved activity and mechanism of these disaggregases. This new MD arrangement is in excellent agreement with recent, extensive biochemical analysis of the MD [33]. It was proposed that the MD works as a molecular toggle switching from a repressed state in which both motif 1 and 2 ends of the propeller are protected, to an active state where motif 2 is deprotected, exposing the binding site for DnaK/Hsp70 [30,32,33]. Our EM reconstructions of repressed, hyperactive and wild type ClpB reveal a lever-like movement of the MD that switches from the repressed state with head-to-tail motif 1-motif 2 binding between adjacent subunits, to a mobile, activated state with motif 2 free and available for binding to DnaK (Figure 7A). The wild type conformation is intermediate between these states and thus poised for switching.

Our data thus explain the critical role of motif 1, which regulates the accessibility of motif 2 and consequently ClpB activity. Confirming its important regulatory role, deletion of motif 1 results in hyperactive ATPase and unfolding activity of ClpB-ΔM1 as well as cell toxicity (Figure 5), representing key characteristics of the hyperactive state [33]. Moreover, our maps suggest that motif 1, through its contacts with either the adjacent motif 2 or AAA-1, plays a key role in direct communication between neighbouring subunits, which must therefore act in a coordinated manner.

It has become clear that AAA+ proteins are highly dynamic molecular motors unlikely to exist in a homogeneous structural state. Therefore we generated asymmetric reconstructions of ClpB. Although the resolution of the asymmetric structures is not sufficient to support a detailed mechanistic model, these reconstructions provide the first visualization of the MD conformational flexibility that was inferred from biochemical analysis [20,33,34]. The asymmetric structures show that the MD orientation varies around the ring occupying the repressed, wild type-like and hyperactive positions described by the symmetrised averages. The variable tilts of MDs observed around the ring suggest that 2 to 4 adjacent subunits are available for DnaK binding in the wild-type versus only 1 in the repressed mutant (Figure 6B,C). This is consistent with the estimated stoichiometry of 2-5 molecules of DnaK per ClpB hexamer required for activation [30,43]. It also suggests that at least 4 subunits must have detached MDs to allow activity, perhaps through movements of the AAA+ domains, in agreement with the number of ClpX subunits that hydrolyze ATP in a coordinated manner to unfold GFP in single molecule experiments [50.] Moreover, we calculated an ADP binding stoichiometry of 4 for both wild type and mutants (Figure 6-supplement 3), which indicates that although ATP hydrolysis is strongly affected, detachment of the MD does not change the nucleotide binding.

The cryo EM reconstruction of wild-type ClpB suggests that the various MD conformations exist only transiently, poised between hyperactive and repressed states, with the balance shifted slightly towards repressive motif 1-motif 2 contacts (Figure 2). DnaK binding to an accessible motif 2 stabilizes the MD in a tilted conformation, thereby in turn breaking the repressive contacts with MDs in neighbouring subunits. Thus, an initial encounter of DnaK will facilitate DnaK binding in the neighbouring MDs. In this model, breakage or formation of motif 1-motif 2 contacts provides a mechanistic basis for signalling DnaK binding or

dissociation in a wavelike manner around the ClpB ring. (Figure 7B). The model predicts spatial proximity of multiple DnaK molecules, which is the case for aggregated but not soluble DnaK substrates, directing ClpB activity specifically to protein aggregates. Moreover, the activation of ClpB by DnaK binding, combined with movements of the highly mobile N domain, might act to deliver the substrate to the channel entrance, where it would be engaged for threading, unfolding and consequent extraction from the aggregate.

Material and methods

Strains, plasmids and proteins

E. coli strains used were derivatives of MC4100. Mutant derivatives of ClpB/BAP were generated by PCR mutagenesis and standard cloning techniques in pDS56 and were verified by sequencing. Wild type and mutant ClpB were purified using Ni-IDA (Macherey-Nagel) and size exclusion chromatography (Superdex S200, Amersham) following standard protocols. Purifications of DnaK, DnaJ, GrpE, ClpP, Luciferase and Casein-YFP were performed as described previously [33]. Pyruvate kinase and α–casein were purchased from Sigma. Protein concentrations were determined with the Bio-Rad Bradford assay.

Electron microscopy of negatively stained and vitrified specimens

BAP(HAP)-ClpP complexes were formed in 20 mM Tris-HCl, pH 7.5, 20 mM KCl, 15 mM $MgCl_2$, 1 mM DTT and 2 mM ATPγS. Proteins were applied to glow-discharged carbon coated grids (EM sciences), previously coated with 5 kDa poly-lysine (Sigma-Aldrich) to positively charge the surface. Samples were stained with 2% uranyl acetate.

For cryo-EM imaging, BAPtrap-ClpP was applied to holey carbon grids coated with a thin carbon film and pretreated with poly-lysine while ClpB specimens were loaded onto lacey carbon grids. Cryo-EM specimens were vitrified in a Vitrobot (FEI). Images were recorded on a 4k Gatan CCD camera at a magnification of 50,000× for negatively stained specimens (pixel size 2.2 Å; underfocus range: 0.5-1.2 µm) and of 80,000× for cryo specimens (pixel size 1.4 Å; underfocus range: 1.5 µM-4 µm). All data were collected on a Tecnai F20 FEG operated at 200 kV under low dose conditions.

Single particle processing

The contrast transfer function (CTF) for each CCD frame was determined with CTFFIND3 [51] and corrected by phase flipping using Bshow1.6 [52]. Side views of BAP-ClpP 2:2 complexes were manually picked using Boxer [53] and extracted into 256×256 boxes. The boxed particles were band-pass filtered between 300 and 10 Å for the negative stain dataset and between 300 and 5 Å for the cryo dataset. They were then normalized to the same mean and standard deviation. Particles were initially aligned to the total sum of 10-20 vertically oriented particles using SPIDER [54]. Individual 1:1 BAP-ClpP complexes were extracted with circular masks and classified by MSA in IMAGIC-5 [55] to remove images that did not represent BAP-ClpP, yielding 17470 particles of wild type BAP-ClpP, 12588 of BAP-E432A-ClpP, 9436 of BAP-Y503D-ClpP and 12568 of HAP-ClpP. The BAPtrap-ClpP cryo dataset included 4592 particles. At this stage, particles were high-pass filtered to 160 Å and initial class averages of 20-30 images each were obtained by MSA. All alignments of 1:1 BAP-ClpP complexes were done limiting the in-plane rotation to +/- 20°. Upon further classification, 5-10 good classes were used to generate a starting model by angular reconstitution [56]. Alternative starting models were also created by applying 6 fold symmetry to single classes and then using the resultant 3D map, generally composed of three discs corresponding to the three layers of the molecule, to generate an anchor set for Euler angle assignment. A low-resolution density map was independently created for each dataset by angular reconstitution with 6-fold symmetry. Particle orientations were refined in multiple cycles of AP SHC alignment in SPIDER, MSA and angular reconstitution in IMAGIC and the resulting 3D reconstruction, filtered to 30 Å, was used as an initial model for projection matching in SPIDER. By applying a rectangular mask, only the AAA+ layers were refined. After 8-10 cycles of projection matching, using progressively smaller angular sampling steps (4° to 1°) and filtering the 3D to the estimated resolution at each cycle, final structures were generated of the whole complex and their resolution was estimated by Fourier shell correlation with a 0.5 correlation cutoff. Based on cross correlation coefficient, around 70-80% of each dataset was included in the final reconstruction.

The differences between the mutant structures were tested by refining with interchanged starting models. In both cases, the original mutant structure was recovered despite the use of the other map as a starting model for projection matching (Figure 3-supplement 1).

For cryo EM ClpB specimen, the views were randomly oriented and the initial strategy was to extract clearly identifiable side views by MSA and classification. 7606 side views were used to generate a starting model by angular reconstitution, which was refined to 29 Å resolution (Figure 1-supplement 3) by projection matching.

For the reconstructions without imposed symmetry, particle orientations were determined using either the 6-fold symmetrized map filtered to 50 Å or a sphere obtained from the average of all particles as a starting model. Subsequently, particle orientations were refined with ~10 cycles of projection matching without imposed symmetry. The particle orientations were well distributed around the BAP-ClpP central axis (Figure 6-supplement 1). The resolution was estimated by Fourier shell correlation (FSC) at 0.5 (Figure 1-supplement 3).

Atomic Structure Fitting

Docking was done using the crystal structures of *E. coli* ClpB-E432A (current study, PDB code: 4CIU) and *E. coli* ClpB ND (PDB code 1KHY). A homology model of Hsp104, obtained using Phyre2 [57] was used for fitting into the HAP reconstruction.

A hexameric ClpB/Hsp104 AAA-1 ring was modelled on the ClpC hexamer crystal structure (PDB code 3PXG) and was automatically fitted as a rigid body into the symmetrised maps using the UCSF Chimera package [58]. The N-terminal, the middle and the AAA-2 domains were first fitted manually and then local fitting was optimized in Chimera, followed by symmetrisation. In the asymmetric reconstructions, dimers of adjacent ClpB subunits were modelled on crystal structures of ClpX hexamers and fitted as rigid bodies in Chimera.

Biochemical assays

Steady-state ATP hydrolysis rates were determined in buffer A (50 mM Tris pH 7.5, 5 mM $MgCl_2$, 20 mM KCl, 2 mM DTT) as described [34]. ClpB disaggregation activities were determined by following the refolding of aggregated firefly Luciferase according to published protocols [34]. Chaperones were used at the following concentrations: 1 µM ClpB (wild type or derivatives), 1 µM DnaK, 0.2 µM DnaJ, 0.1 µM GrpE. Oligomerisation of ClpB variants was tested as described previously [28,34].

Site-specific labelling of ClpB using 1,5-IAEDANS, 5-([(2-iodoacetyl)amino]ethylamino)naphthalene-1-sulfonic acid (Invitrogen) was performed according to the manufacturers' instructions. The intrinsic tryptophan fluorescence of ClpB variant harbouring a single tryptophan (ClpB*-Q427CW, 1 µM

each) was measured on a Perkin-Elmer LS50B spectrofluorimeter at 25°C in low salt buffer A (50 mM Tris pH 7.5, 5 mM $MgCl_2$, 20 mM KCl, 2 mM DTT). Tryptophan and IAEDANS emission spectra of labeled ClpB variants were recorded in high and low salt buffer A (supplemented with 400 mM KCl or 20 mM KCl, respectively) in the absence or presence of 2 mM nucleotide between 300 and 550 nm at a fixed excitation wavelength of 290 nm. The Förster radius of the Trp-IAEDANS FRET pair was calculated as 22 Å [59].

For formation of disulfide bridges ClpB cysteine variants were first dialyzed to remove DTT. Cysteine oxidation was achieved by adding 25 µM Cu-Phenanthroline to 4 µM ClpB and incubating the mixture for 1 min at room temperature. Oxidation and disulfide bond formation was stopped by addition of 50 mM iodoacetamide and SDS-sample buffer containing 5 mM EDTA. Crosslink products were analyzed by a non-reducing SDS gradient gel (3-8%).

Casein-YFP unfolding and degradation assays were carried out using 6 µM BAP (wild type or variants), 9 µM ClpP and 0.5 µM Casein-YFP. Degradation of Casein-YFP was determined by monitoring YFP fluorescence at 535 nm (excitation wavelength 515 nm) at a Perkin-Elmer LS50B spectrofluorimeter.

Spot tests

E. coli cells harbouring plasmid-encoded clpB alleles were grown in the absence of IPTG overnight at 30°C. Serial dilutions were prepared, spotted on LB-plates containing different IPTG concentrations and incubated for 24 h at 37°C.

Isothermal titration calorimetry

ClpB wild type and variants were extensively dialyzed against low salt buffer A (50 mM Tris (pH 7.5), 25 mM KCl, 20 mM $MgCl_2$, 5% glycerol). Isothermal titration calorimetry (ITC) was performed using an ITC calorimeter (iTC200Microcalorimeter, MicroCal). Consecutive injections of nucleotide into a 300 µl cell containing ClpB were performed after sample equilibration at 30°C. Integration and fitting of ITC data were performed using ORIGIN software (GE). ClpB and ADP concentrations were determined by UV absorbance at 280 nm.

Hydrogen-exchange experiments

HX-MS experiments were performed similar to those described earlier [33]. Briefly, ClpB (100 pmol), BAP (100 pmol) or BAP-ClpP complex (100 pmol and 200 pmol

respectively) were incubated for 3 min at 30°C in low salt buffer A (50 mM Tris, pH 7.5, 25 mM KCl, 20 mM $MgCl_2$, 2 mM DTT) in presence of ATP or ATP□S and diluted 20-fold into D_2O-based MDH buffer to initiate amide proton-deuteron exchange. The exchange reaction was stopped after 1 min by the addition of 1 volume of ice-cold quench buffer (0.4 M K-phosphate buffer, pH 2.2). Quenched samples were immediately injected into the HPLC setup, with (peptide analysis) or without (full length protein analysis) online peptic digest, and analysed on an electrospray ionization quadrupole time-of-flight mass spectrometer (QSTAR Pulsar, Applied Biosystems) as described in Rist et al, 2003[60]. Analysis of deuteron incorporation into peptide was performed by using AnalystQS software (Applied Biosystems/MDS SCIEX).

Acknoledgments

We thank Elena Orlova for help in image processing, Christos Savva for EM technical assistance, David Houldershaw for computing support and the Birkbeck EM group for useful discussions. This work was funded by Wellcome Trust grants 089050 and 079605 to H. Saibil. E. Kummer was supported by the Hartmut Hoffmann-Berling International Graduate School of Molecular and Cellular Biology. Y. Oguchi was supported by a Humboldt fellowship.

Accession Numbers

The EM maps have been deposited in the 3D-EM database (www.emdatabank.org) with accession codes EMD-2555 (BAP-E432A C6), EMD-2556 (BAP-E432A C1), EMD-2557 (BAP wild type C6), and EMD-2558 (BAP wild type C1), EMD-2559 (BAP-Y503D C6), EMD-2560 (BAP-Y503D C1), EMD-2561 (HAP), EMD-2562 (BAPtrap cryo) and EMD-2563 (ClpB wild type cryo). The corresponding FSC curves have also been deposited.

References

1. Doyle, S.M. & Wickner, S. Hsp104 and ClpB: protein disaggregating machines. *Trends in Biochemical Sciences* **34**, 40-8 (2009). doi: 10.1016/j.tibs.2008.09.010.
2. Glover, J.R. & Lindquist, S. Hsp104, Hsp70, and Hsp40: a novel chaperone system that rescues previously aggregated proteins. *Cell* **94**, 73-82 (1998). doi: 10.1016/S0092-8674(00)81223-4
3. Goloubinoff, P., Mogk, A., Zvi, A.P., Tomoyasu, T. & Bukau, B. Sequential mechanism of solubilization and refolding of stable protein aggregates by a bichaperone network. *Proceedings of the National Academy of Sciences of the United States of America* **96**, 13732-7 (1999). doi: 10.1073/pnas.96.24.13732
4. Haslberger, T., Bukau, B. & Mogk, A. Towards a unifying mechanism for ClpB/Hsp104-mediated protein disaggregation and prion propagation. *Biochemistry and cell biology = Biochimie et biologie cellulaire* **88**, 63-75 (2010). doi: 10.1139/o09-118.
5. Motohashi, K., Watanabe, Y., Yohda, M. & Yoshida, M. Heat-inactivated proteins are rescued by the DnaK.J-GrpE set and ClpB chaperones. *Proceedings of the National Academy of Sciences of the United States of America* **96**, 7184-9 (1999). doi: 10.1073/pnas.96.13.7184
6. Zolkiewski, M. ClpB cooperates with DnaK, DnaJ, and GrpE in suppressing protein aggregation. A novel multi-chaperone system from Escherichia coli. *The Journal of biological chemistry* **274**, 28083-6 (1999). doi: 10.1074/jbc.274.40.28083
7. Mogk, A. et al. Identification of thermolabile Escherichia coli proteins: prevention and reversion of aggregation by DnaK and ClpB. *The EMBO journal* **18**, 6934-49 (1999). doi: 10.1093/emboj/18.24.6934
8. Parsell, D.A., Kowal, A.S., Singer, M.A. & Lindquist, S. Protein disaggregation mediated by heat-shock protein Hsp104. *Nature* **372**, 475-8 (1994). doi:10.1038/372475a0
9. Haslberger, T. et al. Protein disaggregation by the AAA+ chaperone ClpB involves partial threading of looped polypeptide segments. *Nature structural & molecular biology* **15**, 641-50 (2008). doi: 10.1038/nsmb.1425.
10. Kim, Y.I., Burton, R.E., Burton, B.M., Sauer, R.T. & Baker, T.A. Dynamics of substrate denaturation and translocation by the ClpXP degradation machine. *Molecular Cell* **5**, 639-48 (2000). doi: 10.1016/S1097-2765(00)80243-9
11. Lum, R., Tkach, J.M., Vierling, E. & Glover, J.R. Evidence for an unfolding/threading mechanism for protein disaggregation by Saccharomyces cerevisiae Hsp104. *The Journal of biological chemistry* **279**, 29139-46 (2004). , doi: 10.1074/jbc.M403777200

12. Tessarz, P., Mogk, A. & Bukau, B. Substrate threading through the central pore of the Hsp104 chaperone as a common mechanism for protein disaggregation and prion propagation. *Molecular Microbiology* **68**, 87-97 (2008). doi: 10.1111/j.1365-2958.2008.06135.x.

13. Weber-Ban, E.U., Reid, B.G., Miranker, A.D. & Horwich, A.L. Global unfolding of a substrate protein by the Hsp100 chaperone ClpA. *Nature* **401**, 90-3 (1999). doi:10.1038/43481

14. Weibezahn, J. et al. Thermotolerance requires refolding of aggregated proteins by substrate translocation through the central pore of ClpB. *Cell* **119**, 653-65 (2004). doi: 10.1016/j.cell.2004.11.027

15. Erzberger, J.P. & Berger, J.M. Evolutionary relationships and structural mechanisms of AAA+ proteins. *Annual Review of Biophysics and Biomolecular Structure* **35**, 93-114 (2006). doi: 10.1146/annurev.biophys.35.040405.101933

16. Ogura, T. & Wilkinson, A.J. AAA+ superfamily ATPases: common structure--diverse function. *Genes to cells : devoted to molecular & cellular mechanisms* **6**, 575-97 (2001). doi: 10.1046/j.1365-2443.2001.00447.x

17. Bochtler, M. et al. The structures of HsIU and the ATP-dependent protease HsIU-HsIV. *Nature* **403**, 800-5 (2000). doi:10.1038/35001629

18. Glynn, S.E., Martin, A., Nager, A.R., Baker, T.A. & Sauer, R.T. Structures of asymmetric ClpX hexamers reveal nucleotide-dependent motions in a AAA+ protein-unfolding machine. *Cell* **139**, 744-56 (2009). doi: 10.1016/j.cell.2009.09.034

19. Wang, F. et al. Structure and mechanism of the hexameric MecA-ClpC molecular machine. *Nature* **471**, 331-5 (2011). doi: 10.1038/nature09780

20. Lee, S. et al. The structure of ClpB: a molecular chaperone that rescues proteins from an aggregated state. *Cell* **115**, 229-40 (2003). doi: 10.1016/S0092-8674(03)00807-9

21. Lee, S., Sielaff, B., Lee, J. & Tsai, F.T. CryoEM structure of Hsp104 and its mechanistic implication for protein disaggregation. *Proceedings of the National Academy of Sciences of the United States of America* **107**, 8135-40 (2010). doi: 10.1073/pnas.1003572107.

22. Wendler, P. et al. Atypical AAA+ subunit packing creates an expanded cavity for disaggregation by the protein-remodeling factor Hsp104. *Cell* **131**, 1366-77 (2007). doi: 10.1016/j.cell.2007.10.047

23. Wendler, P. et al. Motor mechanism for protein threading through Hsp104. *Molecular Cell* **34**, 81-92 (2009). doi: 10.1016/j.molcel.2009.02.026.

24. Gai, D., Zhao, R., Li, D., Finkielstein, C.V. & Chen, X.S. Mechanisms of conformational change for a replicative hexameric helicase of SV40 large tumor antigen. *Cell* **119**, 47-60 (2004). doi: 10.1016/j.cell.2004.09.017

25. Huyton, T. et al. The crystal structure of murine p97/VCP at 3.6A. *Journal of Structural Biology* **144**, 337-48 (2003). doi: 10.1016/j.jsb.2003.10.007

26. Desantis, M.E. & Shorter, J. The elusive middle domain of Hsp104 and ClpB: location and function. *Biochimica et Biophysica Acta* **1823**, 29-39 (2012). doi: 10.1016/j.bbamcr.2011.07.014.

27. Kedzierska, S., Akoev, V., Barnett, M.E. & Zolkiewski, M. Structure and function of the middle domain of ClpB from Escherichia coli. *Biochemistry* **42**, 14242-8 (2003). doi: 10.1021/bi035573d

28. Mogk, A. et al. Roles of individual domains and conserved motifs of the AAA+ chaperone ClpB in oligomerization, ATP hydrolysis, and chaperone activity. *The Journal of biological chemistry* **278**, 17615-24 (2003). doi: 10.1074/jbc.M209686200

29. Miot, M. et al. Species-specific collaboration of heat shock proteins (Hsp) 70 and 100 in thermotolerance and protein disaggregation. *Proceedings of the National Academy of Sciences of the United States of America* **108**, 6915-20 (2011). doi: 10.1073/pnas.1102828108.

30. Seyffer, F. et al. Hsp70 proteins bind Hsp100 regulatory M domains to activate AAA+ disaggregase at aggregate surfaces. *Nature structural & molecular biology* **19**, 1347-55 (2012). doi: 10.1038/nsmb.2442.

31. Sielaff, B. & Tsai, F.T. The M-domain controls Hsp104 protein remodeling activity in an Hsp70/Hsp40-dependent manner. *Journal of Molecular Biology* **402**, 30-7 (2010). doi: 10.1016/j.jmb.2010.07.030.

32. Rosenzweig, R., Moradi, S., Zarrine-Afsar, A., Glover, J.R. & Kay, L.E. Unraveling the mechanism of protein disaggregation through a ClpB-DnaK interaction. *Science* **339**, 1080-3 (2013). doi: 10.1126/science.1233066.

33. Oguchi, Y. et al. A tightly regulated molecular toggle controls AAA+ disaggregase. *Nature structural & molecular biology* **19**, 1338-46 (2012). doi: 10.1038/nsmb.2441.

34. Haslberger, T. et al. M domains couple the ClpB threading motor with the DnaK chaperone activity. *Molecular Cell* **25**, 247-60 (2007). doi: 10.1016/j.molcel.2006.11.008

35. Lipinska, N. et al. Disruption of ionic interactions between the nucleotide binding domain 1 (NBD1) and middle (M) domain in Hsp100 disaggregase unleashes toxic hyperactivity and partial independence from Hsp70. *The Journal of biological chemistry* **288**, 2857-69 (2013). doi: 10.1074/jbc.M112.387589.

36. Mizuno, S., Nakazaki, Y., Yoshida, M. & Watanabe, Y.H. Orientation of the amino-terminal domain of ClpB affects the disaggregation of the protein. *The FEBS journal* **279**, 1474-84 (2012). doi: 10.1111/j.1742-4658.2012.08540.x.

37. Effantin, G., Ishikawa, T., De Donatis, G.M., Maurizi, M.R. & Steven, A.C. Local and global mobility in the ClpA AAA+ chaperone detected by cryo-electron

microscopy: functional connotations. *Structure* **18**, 553-62 (2010). doi: 10.1016/j.str.2010.02.016.

38. Parsell, D.A., Kowal, A.S. & Lindquist, S. Saccharomyces cerevisiae Hsp104 protein. Purification and characterization of ATP-induced structural changes. *The Journal of biological chemistry* **269**, 4480-7 (1994).

39. Schlothauer, T., Mogk, A., Dougan, D.A., Bukau, B. & Turgay, K. MecA, an adaptor protein necessary for ClpC chaperone activity. *Proceedings of the National Academy of Sciences of the United States of America* **100**, 2306-11 (2003). doi: 10.1073/pnas.0535717100

40. Lee, S., Choi, J.M. & Tsai, F.T. Visualizing the ATPase cycle in a protein disaggregating machine: structural basis for substrate binding by ClpB. *Molecular Cell* **25**, 261-71 (2007). doi: 10.1016/j.molcel.2007.01.002

41. Biter, A.B., Lee, J., Sung, N., Tsai, F.T. & Lee, S. Functional analysis of conserved cis- and trans-elements in the Hsp104 protein disaggregating machine. *Journal of Structural Biology* **179**, 172-80 (2012). doi: 10.1016/j.jsb.2012.05.007

42. Yamasaki, T., Nakazaki, Y., Yoshida, M. & Watanabe, Y.H. Roles of conserved arginines in ATP-binding domains of AAA+ chaperone ClpB from Thermus thermophilus. *The FEBS journal* **278**, 2395-403 (2011). doi: 10.1111/j.1742-4658.2011.08167.x.

43. Desantis, M.E. et al. Conserved Distal Loop Residues in the Hsp104 and ClpB Middle Domain Contact Nucleotide-binding Domain 2 and Enable Hsp70-dependent Protein Disaggregation. *The Journal of biological chemistry* **289**, 848-67 (2014). doi: 10.1074/jbc.M113.520759.

44. del Castillo, U. et al. A quantitative analysis of the effect of nucleotides and the M domain on the association equilibrium of ClpB. *Biochemistry* **50**, 1991-2003 (2011). doi: 10.1021/bi101670s

45. Kon, T. et al. The 2.8 A crystal structure of the dynein motor domain. *Nature* **484**, 345-50 (2012). doi: 10.1038/nature10955.

46. Stinson, B.M. et al. Nucleotide binding and conformational switching in the hexameric ring of a AAA+ machine. *Cell* **153**, 628-39 (2013). doi: 10.1016/j.cell.2013.03.029

47. Cho, C. & Vale, R.D. The mechanism of dynein motility: insight from crystal structures of the motor domain. *Biochimica et Biophysica Acta* **1823**, 182-91 (2012). doi: 10.1016/j.bbamcr.2011.10.009.

48. Moreau, M.J., McGeoch, A.T., Lowe, A.R., Itzhaki, L.S. & Bell, S.D. ATPase site architecture and helicase mechanism of an archaeal MCM. *Molecular Cell* **28**, 304-14 (2007). doi: 10.1016/j.molcel.2007.08.013

49. Yakamavich, J.A., Baker, T.A. & Sauer, R.T. Asymmetric nucleotide transactions of the HslUV protease. *Journal of Molecular Biology* **380**, 946-57 (2008). doi: 10.1016/j.jmb.2008.05.070.
50. Sen, M. et al. The ClpXP protease unfolds substrates using a constant rate of pulling but different gears. *Cell* **155**, 636-46 (2013). doi: 10.1016/j.cell.2013.09.022
51. Mindell, J.A. & Grigorieff, N. Accurate determination of local defocus and specimen tilt in electron microscopy. *Journal of Structural Biology* **142**, 334-347 (2003). doi: 10.1016/S1047-8477(03)00069-8
52. Heymann, J.B. & Belnap, D.M. Bsoft: Image processing and molecular modeling for electron microscopy. *Journal of Structural Biology* **157**, 3-18 (2007). doi: 10.1016/j.jsb.2006.06.006
53. Ludtke, S.J., Baldwin, P.R. & Chiu, W. EMAN: Semiautomated software for high-resolution single-particle reconstructions. *Journal of Structural Biology* **128**, 82-97 (1999). doi: 10.1006/jsbi.1999.4174
54. Frank, J. et al. SPIDER and WEB: Processing and visualization of images in 3D electron microscopy and related fields. *Journal of Structural Biology* **116**, 190-199 (1996). doi: 10.1006/jsbi.1996.0030
55. van Heel, M., Harauz, G., Orlova, E.V., Schmidt, R. & Schatz, M. A new generation of the IMAGIC image processing system. *Journal of Structural Biology* **116**, 17-24 (1996). doi: 10.1006/jsbi.1996.0004
56. van Heel, M. et al. Single-particle electron cryo-microscopy: towards atomic resolution. *Quarterly Reviews of Biophysics* **33**, 307-69 (2000).
57. Kelley, L.A. & Sternberg, M.J. Protein structure prediction on the Web: a case study using the Phyre server. *Nature protocols* **4**, 363-71 (2009). doi: 10.1038/nprot.2009.2.
58. Pettersen, E.F. et al. UCSF Chimera--a visualization system for exploratory research and analysis. *Journal of computational chemistry* **25**, 1605-12 (2004). doi: 10.1002/jcc.20084
59. Jeganathan, S., von Bergen, M., Brutlach, H., Steinhoff, H.J. & Mandelkow, E. Global hairpin folding of tau in solution. *Biochemistry* **45**, 2283-93 (2006). doi: 10.1021/bi0521543
60. Rist, W., Jørgensen, T.J.D., Roepstorff, P., Bukau, B., & Mayer, M.P. Mapping temperature-induced conformational changes in the *Escherichia coli* heat shock transcription factor σ^{32} by amide hydrogen exchange. *Journal of Biological Chemistry*

Figure captions

Figure 1. 3D structure of the symmetrised BAP-ClpP complex. (**A**) Schematic of the complex showing the threading of a polypeptide. ClpB domains are in yellow, N-terminus; red/orange, AAA-1 domain; green, MD and blue/cyan, AAA-2 domain. ClpP is in grey. (**B**) Negative stain EM image (left panel), class averages of 2:2 BAP-ClpP (upper right panel) and cut out 1:1 BAP-ClpP particles (bottom right panel). Scale bars are 150 Å. (**C**) BAP-ClpP structure with a fitted ClpB monomer (left) and central slice with fitted atomic coordinates (right). (**D**) AAA-1 and AAA-2 layers. (**E**) Two adjacent AAA-1 domains from the hexameric fit viewed in the plane of the ring. One monomer is in colour and the other in grey. Residues involved in engineered disulphide bonds are shown as spheres. Residues involved in intermolecular cross-links are labeled. The separation between cross-linking Cα pairs ranges from 8 to 14 Å.

Figure 2. Independently determined maps and fitted hexameric models of HAP-ClpP, BAPtrap-ClpP and ClpB. (**A**) Negative stain EM map of HAP-ClpP. From left to right: surface side-view, AAA-1 layer and AAA-2 layer. The central channel enclosed by the AAA-2 ring is filled with density. (**B**) Cryo EM map of BAP-ClpP formed with the BAP variant that traps the substrate inside. (**C**) Cryo EM map of wild type ClpB alone.

Figure 3. Structures of repressed and hyperactive BAP-ClpP mutants. (**A**) Side view (left) and 35 Å section (right) of the BAP-E432A map with the ClpB hexamer fit. (**B**) Fitting of the BAP-E432A AAA+ rings. (**C**) Side view (left) and 35 Å section of the fitted BAP-Y503D structure. MD is only partially in density and is more tilted than in the wild type and the BAP-E432A repressed mutant. The ND is smeared out as in all BAP forms due to disorder, but has a more vertical orientation in the hyperactive state. (**D**) Fitting of the BAP-Y503D AAA+ rings. The motif 2 region protrudes from the density.

Figure 4. Analysis of MD movements. (**A**) Repressed (red), wild-type (yellow) and hyperactive (green) forms of BAP-ClpP with a fitted subunit. (**B**) Distances (d) are shown between Cα atoms of Q427 (motif 1) and Q502 (motif 2) of neighbouring subunits based on the symmetrised EM reconstructions of wild-type ClpB and MD mutants. (**C**) Fluorescence energy transfer between motif 1 and motif 2 of adjacent ClpB subunits. Emission spectra of ClpB-Q427W-Q502C-IAEDANS in the monomeric (high salt), oligomeric (low salt) and ATP state (2 mM ATP) are shown. Effects of MD mutations on FRET efficiency were determined. The ratio of acceptor to donor fluorescence (derived from the areas under the curves) was calculated as readout for FRET efficiency. (**D**) Intermolecular disulfide crosslinking between MD motif 1 and motif 2 of adjacent subunits. Reduced and oxidized

ClpB-K431C-S499C and repressed (E432A) and hyperactive (Y503D) variants were analyzed by non-reducing SDS-PAGE. Positions of monomers (1) and crosslinked dimers (2), trimers (3), tetramers (4), pentamers (5) and hexamers (6) are indicated. A protein standard is given. CoPhe at 25 µM was used as oxidizing agent.

Figure 5 Deletion of MD motif 1 causes ClpB activation. (**A**) Basal and substrate-stimulated ATPase activities of ClpB wild type and indicated MD deletions were determined in the absence and presence of casein. Relative ATPase activations by casein were calculated (inset). (**B**) Unfolding of Casein-YFP by BAP wild type and indicated MD deletions in the presence of ClpP was monitored by YFP fluorescence. Initial YFP fluorescence was set to 100%. ΔM1: ΔE410-Y455, ΔM2: ΔS456-E520, ΔM1/M2: ΔE410-E520. (**C**) *E. coli ΔclpB* cells expressing the indicated plasmid-encoded *clpB* alleles under control of an IPTG-regulatable promoter were grown overnight at 30°C. Various dilutions (10^{-1}–10^{-7}) were spotted on LB plates containing the indicated IPTG concentration and incubated at 37°C for 24 h.

Figure 6. Variations in MD orientations around the ring. (**A**) Asymmetric reconstructions of repressed BAP-E432A, wild type BAP-ClpP and hyperactive BAP-Y503. (**B**) Side views of the BAP-ClpP wild type structure rotated successively 60°. Red MDs are oriented horizontally and make motif 1 to motif 2 contact as in the repressed state. Yellow MDs have slightly tilted orientations similar to the wild type. Green MDs are tilted as in the hyperactive state. One of the MDs contacts AAA-2 of the same subunit (last right panel). (**C**) Equivalent views of the BAP E432A-ClpP repressed mutant structure. Color code for the MD orientations is the same as above.

Figure 7. Interaction between the ClpB hexamer and DnaK. (**A**) Binding of DnaK is only possible when the MD is tilted (green). DnaK cannot bind when two adjacent MDs occupy a more horizontal position (red) as it would clash with motif 1 of the neighbouring ClpB subunit. (**B**) Cartoon of an opened-out ClpB ring with two DnaK molecules bound. The MDs involved in DnaK binding are shown in green, and those that cannot bind to DnaK are shown in red. Release of the ends of the MD favours activation of adjacent subunits, and the active cluster can move around the ring in a wave-like manner. The model of DnaK binding to the MD is based on the NMR study in ref. 32.

Figure 1 supplement 1 Complex formation between BAP and ClpP does not change MD protection pattern in HX experiments. (**A**) BAP and ClpP form a stable complex during HX experiments causing stabilization of BAP. Protein samples preincubated with ATPγS (BAP, BAP-ClpP) were diluted 20-fold into D_2O buffer and incubated for 60 s before quenching the

proton-deuteron exchange reaction. The mass of full length BAP after deuteron incorporation was determined. Complex formation with ClpP protects 30 amide protons in BAP from exchange. (**B**) ClpB, BAP and BAP-ClpP were incubated with ATPγS and HX values of peptic peptides were determined after 60 s. Peptide 746-754 (*, KKIFRPEFI) includes the ClpP-binding loop of ClpA and is only present in BAP. Relative (%) deuterium incorporation levels are given for each peptide.

Figure 1 supplement 2 The BAP N-terminus is highly mobile. (**A**) Class averages of BAP-ClpP. The arrows indicate the N-terminal (yellow), AAA-1 (red), AAA-2 (blue) and ClpP (black) tiers. (**B**) Eigen images showing that high variance is localized in the N-terminal ring. Scale bars are 50 Å.

Figure 1 supplement 3 Fourier Shell Correlation plots to estimate EM map resolution. For each sample, FSC curves of C6 and C1 reconstructions are plotted together. The C1 curves show lower resolution in each pair. Example class averages are shown in the left column with corresponding re-projections on the right. FSC plots were deposited in the 3D-EM database EM (www.emdatabank.org).

Figure 1 supplement 4 Crystal structure of *E. coli* ClpB and EM based model. (**A**) Superimposed chains of *E. coli* ClpB and *T. thermophilus* crystal structures. For clarity, the N-terminus is not shown. (**B**) Comparison between the ClpB coordinates fitted into the EM maps (in colours) and the ClpB crystal structure (grey). In the EM model the MD is more tilted than in the crystal structures. AAA-2 is rotated by ~25°, and the N-terminus is rotated by 45° in the plane of the ring.

Figure 3 supplement 1 Test of EM map refinements after interchange of starting models.

Figure 4 supplement 1 Contacts between adjacent MDs in the EM model compared to those found in the ClpB crystal structures.

Figure 4 supplement 2 Tryptophan emission spectra of unlabeled ClpB-Q427W-Q502C and of corresponding MD mutants in the monomeric (HS, high salt), oligomeric (LS, low salt) and ATP-loaded state (LS + 2 mM ATP) are given. High salt (400 mM KCl) prevents ClpB oligomerisation.

Figure 6 supplement 1 Plots showing the angular distribution of single particles (red dots) around the Euler sphere for each asymmetric reconstruction. Angle search was done with 2°

sampling. The equatorial band reflects the Euler angle distribution around the BAP-ClpP central axis.

Figure 6 supplement 2 Open and closed conformations of AAA+ domains can be fitted into the asymmetric ClpB map. (**A**) Superimposition of an open (blue) and a closed (grey) nucleotide pocket (ClpX 3HWS). ADP is depicted in green spheres. (**B**) *Eco*ClpB AAA-2 dimers built with open, intermediate and closed conformations based on ClpX crystallographic dimers. (**C**) AAA-1 and AAA-2 layers of asymmetric wild-type ClpB reconstruction plus indication of nucleotide occupancy.

Figure 6 supplement 3 Asymmetric nucleotide binding to ClpB. (**A-D**) Instrumental responses of successive injections of ADP (8.39 mM, 1.92 mM, 5.82 mM and 4.05 mM ADP for ClpB-WT, ClpB-K212A, ClpB-E432A, ClpB-Y503D, respectively) into a solution of ClpB-WT (678 µM), ClpB-K212A (239 µM), ClpB-E432A (467 µM) and ClpB-Y503D (396 µM). The molar ratio of ADP to ClpB hexamer is indicated. Raw isothermal titration calorimetry data are shown. Integrated data after base-line-correction and fitting to the respective binding isotherms to a single-site binding model are given (lower panel). The number of ADP binding sites was calculated.

Table 1: X-ray data collection and refinement statistics

Protein	ClpB E279A/E432A/E678A (SeMet) + ATP
Wavelength (Å)	0.9794
Space group	$P6_5$
Unit cell (Å,°)	127.34, 127.34, 119.86, 90, 90, 120
Molecules	1
Resolution (Å)	81.15-3.50 (3.69-3.50)
Reflections measured	202965
Unique reflections	14024
Rmerge	8.8 (53.2)
Rpim	3.0 (14.9)
I/σI	16.8 (5.4)
Completeness (%)	99.9 (100)
Redundancy	14.5 (14.8)
Rwork/Rfree (%)	22.5/24.5
Protein residues	657 (5257 atoms)
ADP	2
Rmsd bond lengths (Å)	0.004
Rmsd bond angles (°)	0.94
Average B-Factor Protein	99.6
Average B-Factor ADP	87.7
Ramachandran plot statistics	
Favored (%)	95.5
Allowed (%)	4.1
Generous (%)	0.4
Disallowed (%)	0
PDB entry code	4CIU

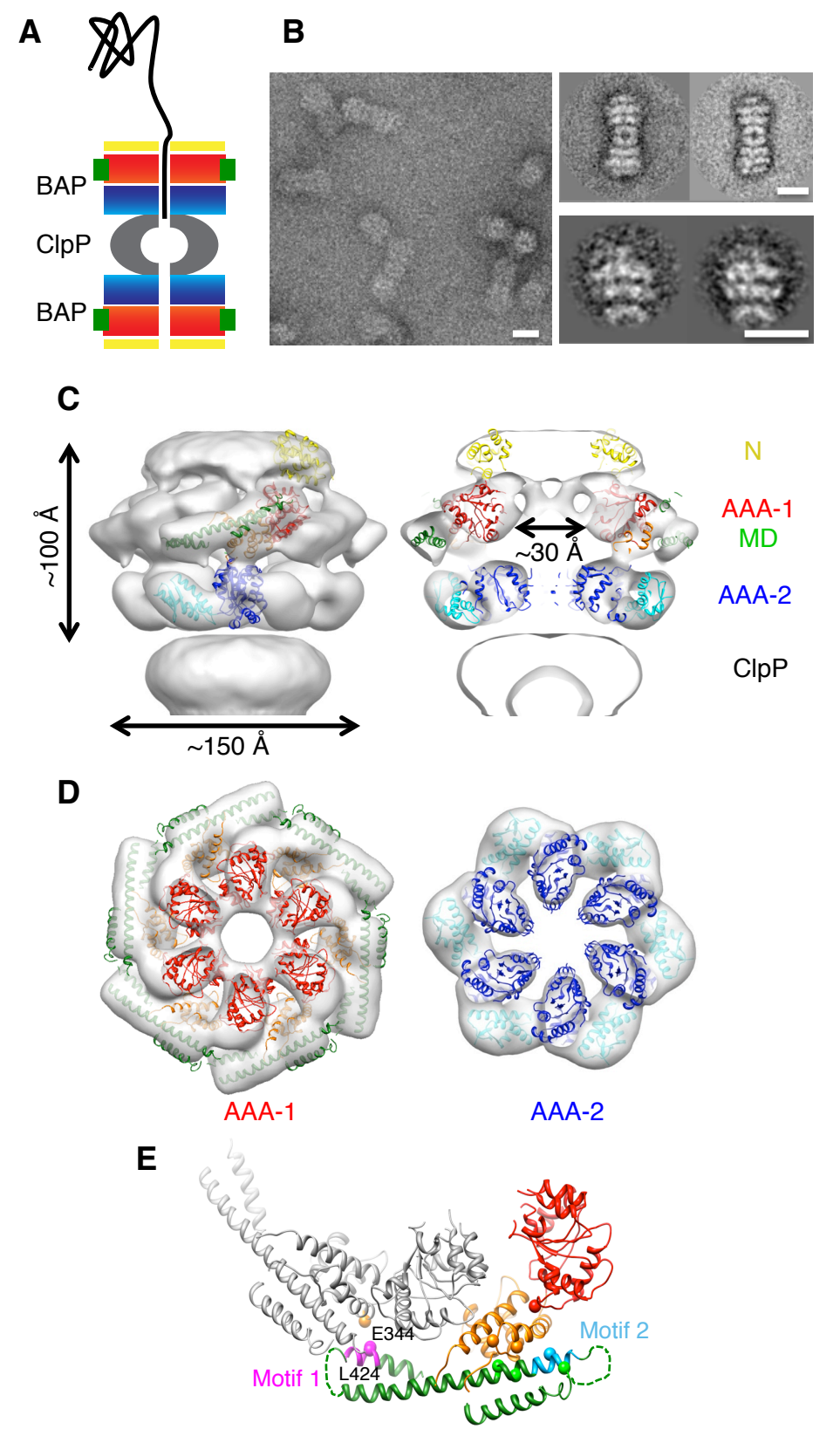
A
BAP
ClpP
BAP
B
C
~100 Å
~150 Å
~30 Å
N
AAA-1
MD
AAA-2
ClpP
D
AAA-1
AAA-2
E
E344
L424
Motif 1
Motif 2

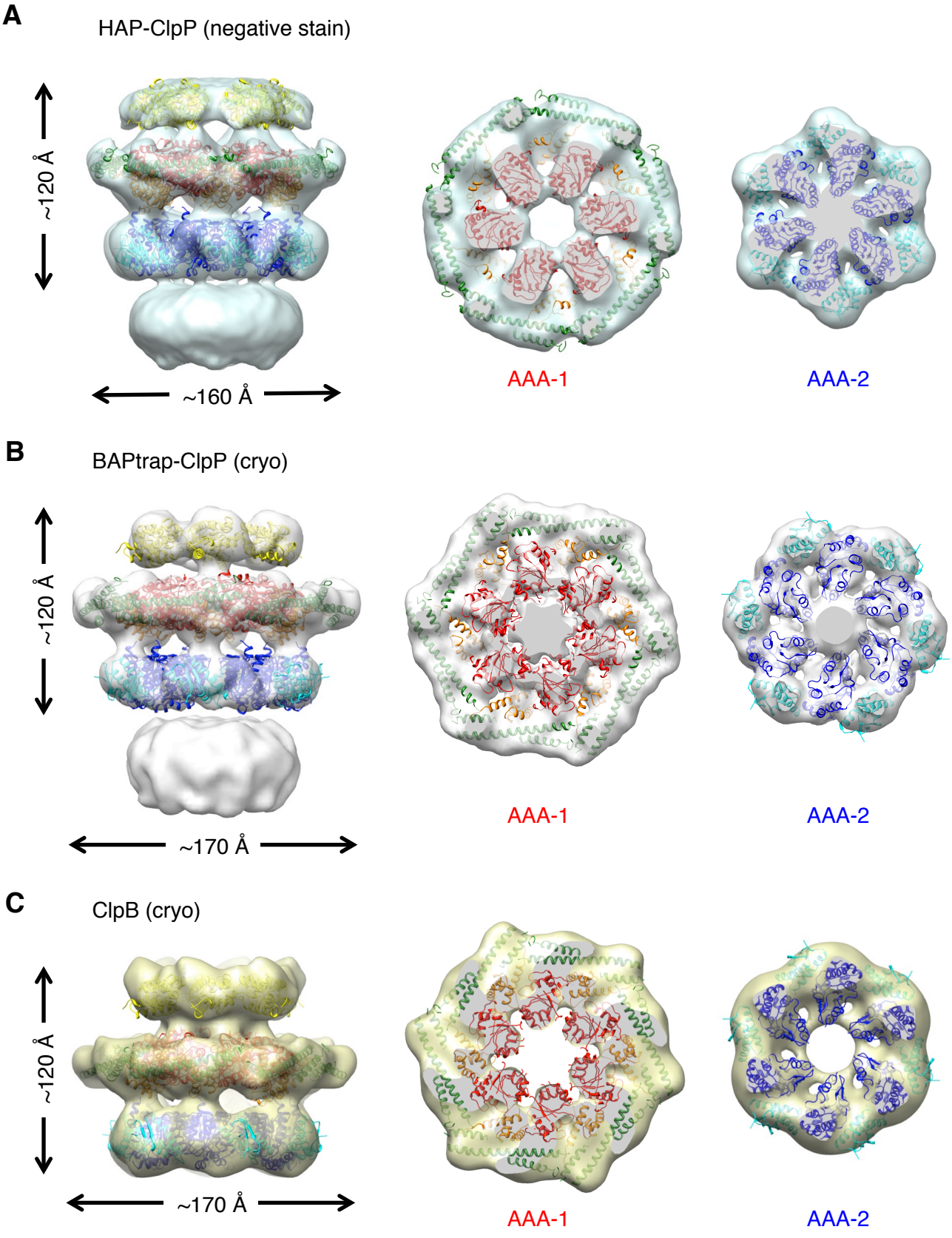
A
HAP-ClpP (negative stain)
~120 Å
~160 Å
AAA-1
AAA-2
B
BAPtrap-ClpP (cryo)
~120 Å
~170 Å
AAA-1
AAA-2
C
ClpB (cryo)
~120 Å
~170 Å
AAA-1
AAA-2

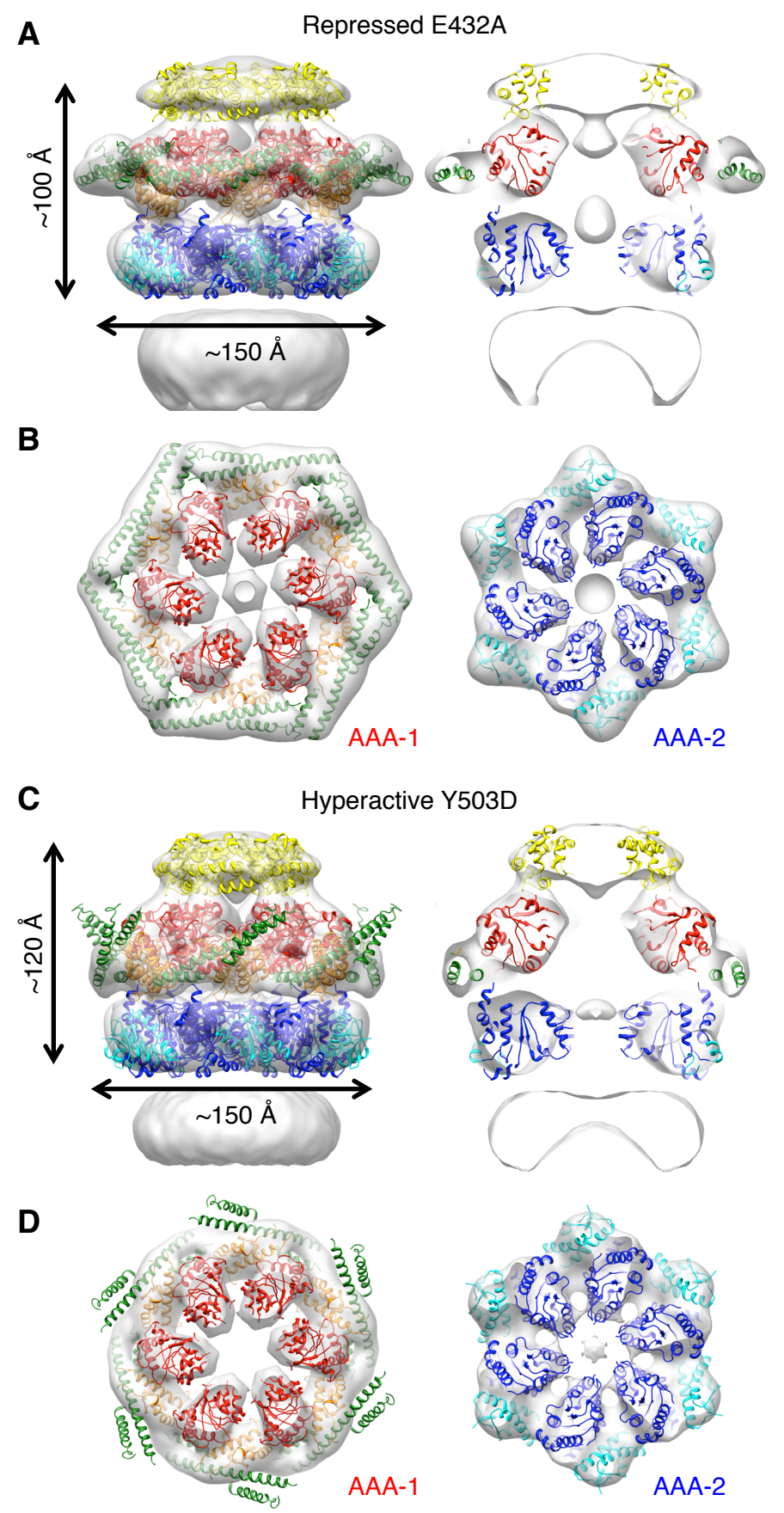
A
Repressed E432A
~100 Å
~150 Å
B
AAA-1
AAA-2
C
Hyperactive Y503D
~120 Å
~150 Å
D
AAA-1
AAA-2

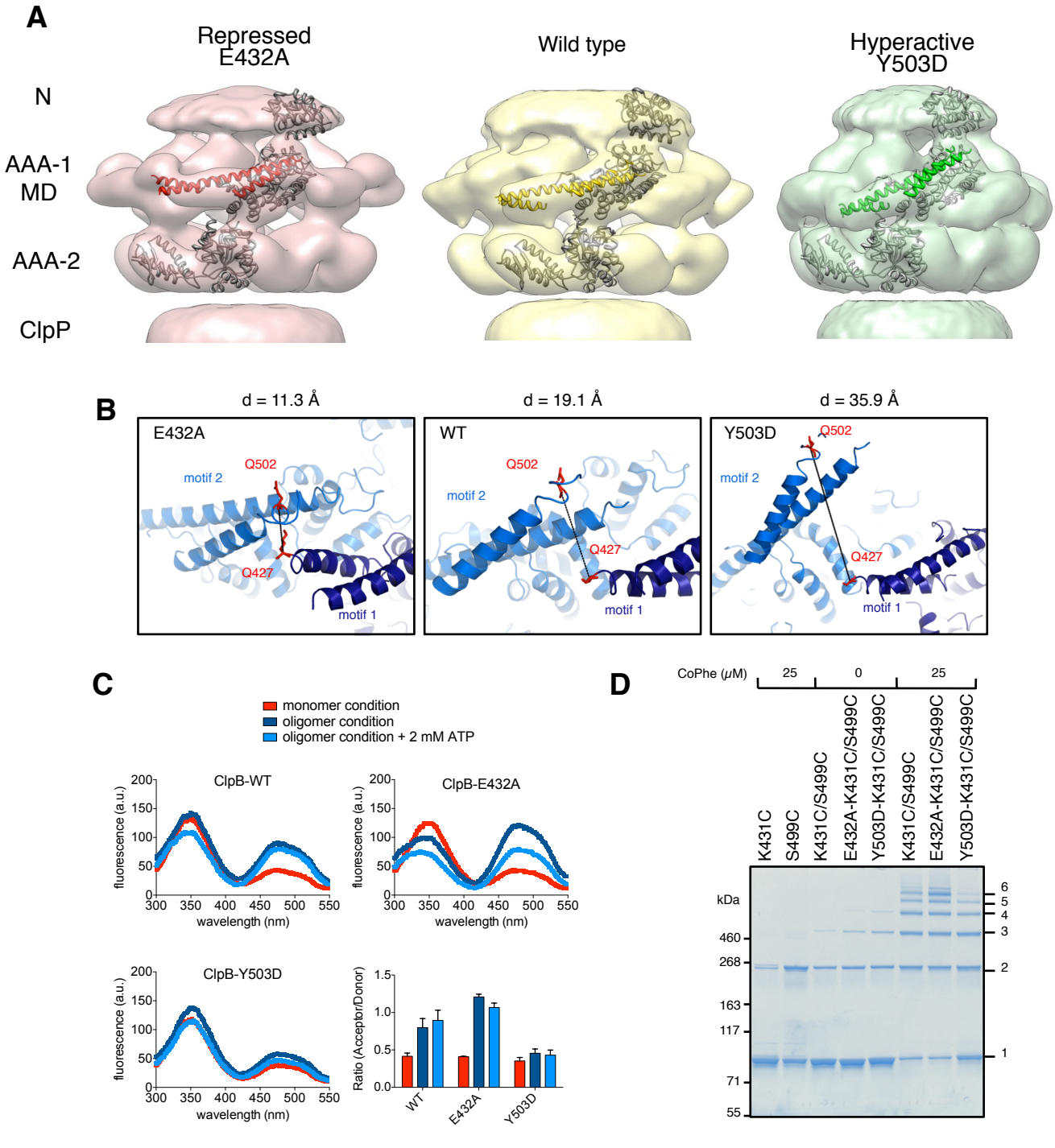
A
Repressed
E432A
Wild type
Hyperactive
Y503D
N
AAA-1
MD
AAA-2
ClpP
B
d = 11.3 Å
d = 19.1 Å
d = 35.9 Å
E432A
WT
Y503D
Q502
Q427
motif 2
motif 1
C
monomer condition
oligomer condition
oligomer condition + 2 mM ATP
ClpB-WT
ClpB-E432A
ClpB-Y503D
fluorescence (a.u.)
wavelength (nm)
Ratio (Acceptor/Donor)
WT
E432A
Y503D
D
CoPhe (μM)
25
0
25
K431C
S499C
K431C/S499C
E432A-K431C/S499C
Y503D-K431C/S499C
kDa
460
268
163
117
71
55
6
5
4
3
2
1

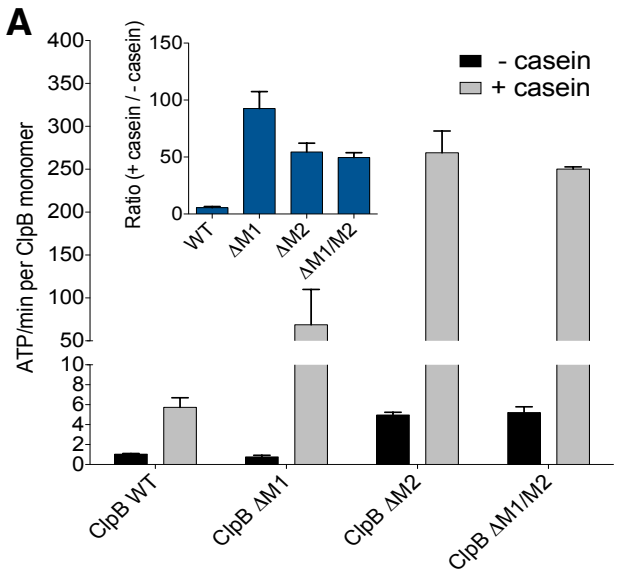
A
ATP/min per ClpB monomer
400
350
300
250
200
150
100
50
10
8
6
4
2
0
- casein
+ casein
Ratio (+ casein / - casein)
150
100
50
0
WT
ΔM1
ΔM2
ΔM1/M2
ClpB WT
ClpB ΔM1
ClpB ΔM2
ClpB ΔM1/M2

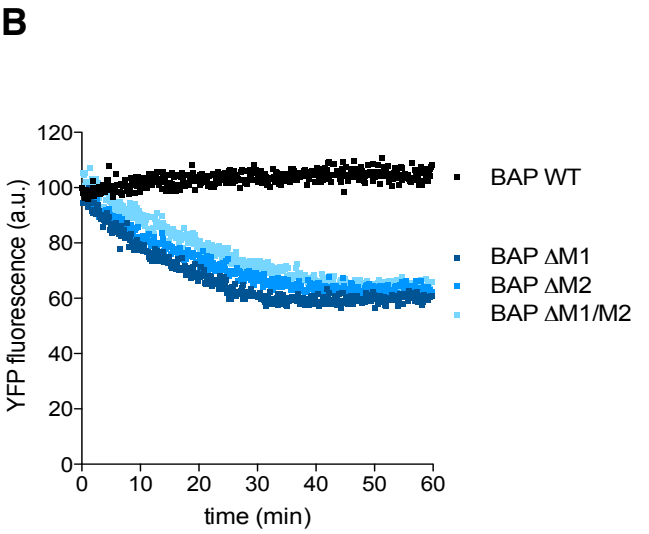
B
YFP fluorescence (a.u.)
120
100
80
60
40
20
0
0
10
20
30
40
50
60
time (min)
BAP WT
BAP ΔM1
BAP ΔM2
BAP ΔM1/M2

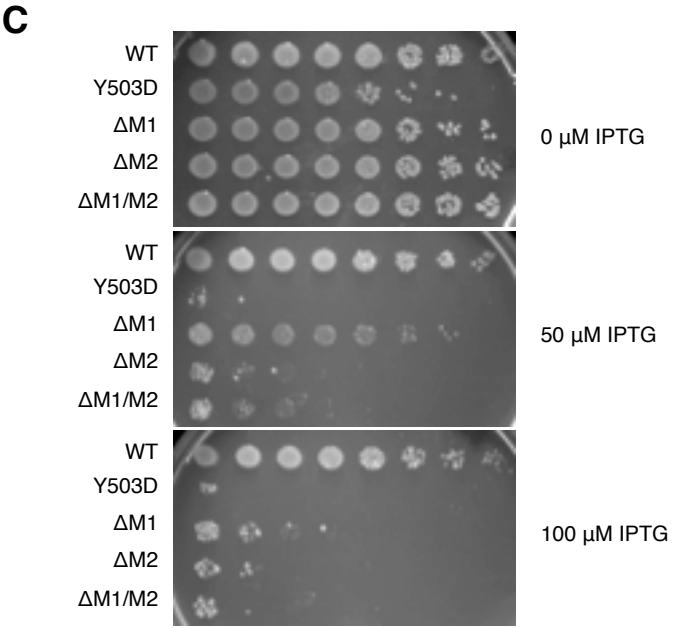
C
WT
Y503D
ΔM1
ΔM2
ΔM1/M2
0 μM IPTG
WT
Y503D
ΔM1
ΔM2
ΔM1/M2
50 μM IPTG
WT
Y503D
ΔM1
ΔM2
ΔM1/M2
100 μM IPTG

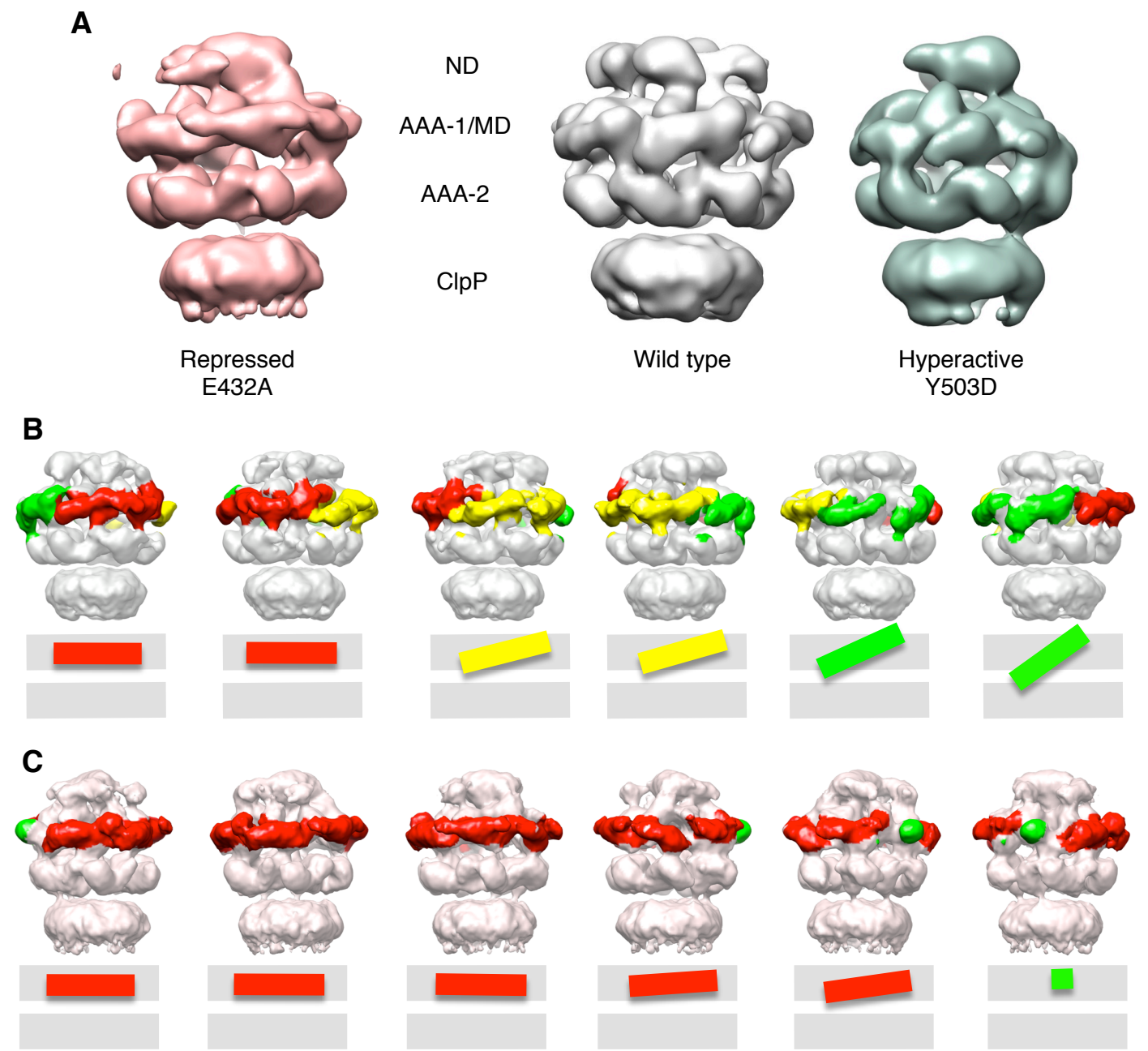
A
ND
AAA-1/MD
AAA-2
ClpP
Repressed
E432A
Wild type
Hyperactive
Y503D
B
C

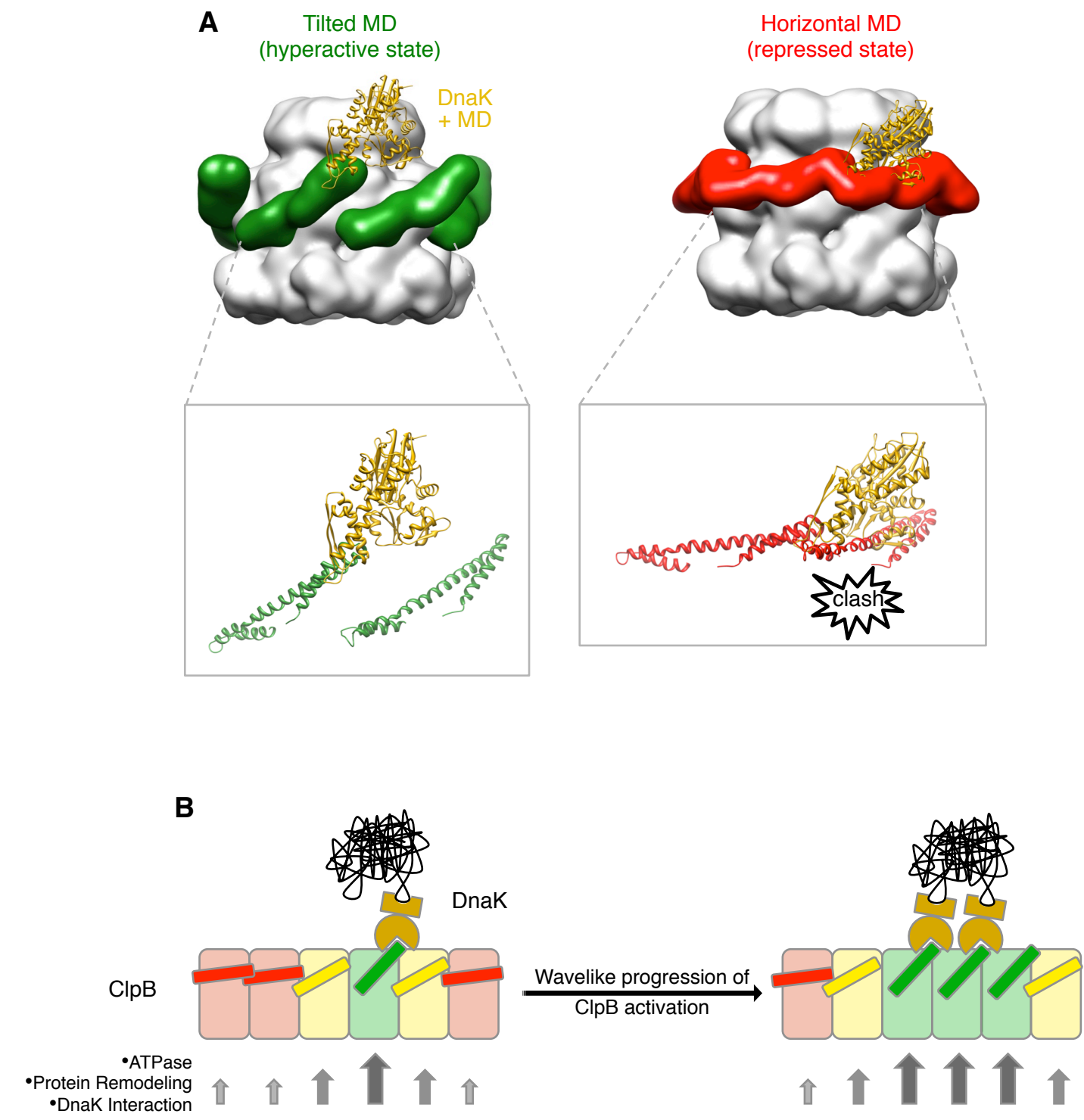
A
Tilted MD
(hyperactive state)
Horizontal MD
(repressed state)
DnaK
+ MD
clash
B
DnaK
ClpB
Wavelike progression of
ClpB activation
•ATPase
•Protein Remodeling
•DnaK Interaction